Available online at www.sciencedirect.com
SCIENCE DIRECT®
ELSEVIER
Nuclear Instruments and Methods in Physics Research A 539 (2005) 622–639
NUCLEAR INSTRUMENTS & METHODS IN PHYSICS RESEARCH Section A
www.elsevier.com/locate/nima

FUNSPIN polarized cold-neutron beam at PSI

J. Zejma[a,*], G. Ban[b], M. Beck[c], A. Białek[d], K. Bodek[a], G. Frei[e], Ch. Hilbes[e], G. Kühne[e], P. Gorel[b,e], K. Kirch[e], St. Kistryn[a], A. Kozela[d], M. Kuźniak[a], A. Lindroth[c], O. Naviliat-Cuncic[b], J. Pulut[a,e], N. Severijns[c], E. Stephan[f]

[a]*Instytut Fizyki, Uniwersytet Jagielloński, ul Reymonta 4, Kraków PL-30059, Poland*
[b]*Laboratoire de Physique Corpusculaire, Caen, France*
[c]*Instituut voor Kern- en Stralingsfysica, Katholieke Universiteit Leuven, Belgium*
[d]*Instytut Fizyki Jądrowej Polskiej Akademii Nauk, Kraków, Poland*
[e]*Paul Scherrer Institut, Villigen, Switzerland*
[f]*Instytut Fizyki, Uniwersytet Śląski, Katowice, Poland*

Received 10 August 2004; received in revised form 5 November 2004; accepted 9 November 2004
Available online 8 December 2004

Abstract

Properties of the cold-neutron beam at the FUNSPIN facility of the SINQ neutron source of the Paul Scherrer Institute, Villigen, Switzerland were investigated. The measured flux density $\Phi = (2.46 \pm 0.04) \times 10^8\,[\mathrm{cm^2\,s\,mA}]^{-1}$, the wavelength averaged mean polarization around the beam axis $P_A = (95.29 \pm 0.04)\%$ and the mean polarization over the full beam cross-section $P = [89.75 \pm 0.01\ (\mathrm{stat}) \pm 1.0\ (\mathrm{syst})]\%$ are the main attributes of this powerful facility for fundamental particle physics experiments with slow neutrons.

PACS: 28.20.−v; 29.90.+r; 81.90.+c

Keywords: Polarized neutrons; Cold neutrons; Neutron polarimetry; Neutron radiography

1. Introduction

Polarized slow neutron beams are commonly used to investigate various problems in, e.g. solid-state physics and medicine as well as in fundamental physics. Cold-neutron beams are especially important—they are advantageous over thermal ones because of the higher spatial neutron density available.

The Swiss Spallation Neutron Source (SINQ) [1] installed at the Paul Scherrer Institute in Villigen, Switzerland, provides both thermal and cold neutrons. The FUNSPIN cold-neutron facility (Channel 51) contains a supermirror polarizer

*Corresponding author. Tel.: +48 12 663 5558; fax: +48 12 634 2038.
E-mail address: zejma@if.uj.edu.pl (J. Zejma).

0168-9002/$ - see front matter © 2004 Elsevier B.V. All rights reserved.
doi:10.1016/j.nima.2004.11.004

and delivers a highly polarized neutron beam. The construction of this facility was described in detail elsewhere [2]. The aim of this study is to provide information about the FUNSPIN cold-neutron beam needed for fundamental physics experiments and for neutron radiography measurements.

Fundamental physics experiments require beams having well known properties since the studied effects are, in general, very small. In particular, the beam polarization should be high and known with good accuracy. The first experiment approved for the FUNSPIN polarized cold-neutron beam line attempts to measure the transverse electron polarization in correlation with the neutron spin and electron momentum [3]. A non-zero value of the so-called R-correlation coefficient [4] would be a sign of time reversal symmetry non-conservation in the weak interaction, which in turn would indicate the existence of physics beyond the Standard Model [5]. To determine R experimentally one has to know the neutron beam polarization and the vector product of momentum and spin of the electrons originating from the neutron decay. The analysis of the electron spin and momentum is described in Ref. [6], while this paper is devoted to a thorough study of the polarization of the FUNSPIN cold-neutron beam.

The high interaction cross-sections of cold neutrons with matter makes them a useful tool for studies of macroscopic samples by neutron radiography [7]. The beam uniformity was investigated since it influences strongly the quality of the obtained images.

In this paper the results of a systematic scan of the beam intensity (Section 2) and polarization (Section 3) are presented. We will also compare the neutron-density and polarization spectra measured after 3 years of operation of the facility with those measured at the very beginning to examine changes caused by possible aging effects of the apparatus.

2. Intensity and geometrical properties of the neutron beam

A schematic view of the FUNSPIN facility is shown in Fig. 1. Neutrons leave a moderator in the cold neutron source and are transported to the experimental area through a 12 m long, evacuated neutron guide equipped with supermirror walls. A 1.6 m long section just after the main shutter houses a multi-slit supermirror polarizer. Polarized neutrons are then spatially compressed by a 5.5 m long condenser. The last 1.4 m long part of the condenser is a radio frequency spin flipper section. At the end of the guide the beam has a rectangular cross-section of $40 \times 150\,\mathrm{mm}^2$ [2]. The guide is closed with a 125 μm thick zirconium window. Just behind this window a fail-safe shutter is placed followed by a collimator which is specific for the R-correlation experiment. The 450 mm long, 45 mm wide and 145 mm high collimator channel is lined with ^{6}LiF polymer foils fixed to borated epoxy plates. It is surrounded by lead and concrete bricks and finally, by large concrete blocks. As in the case of the neutron

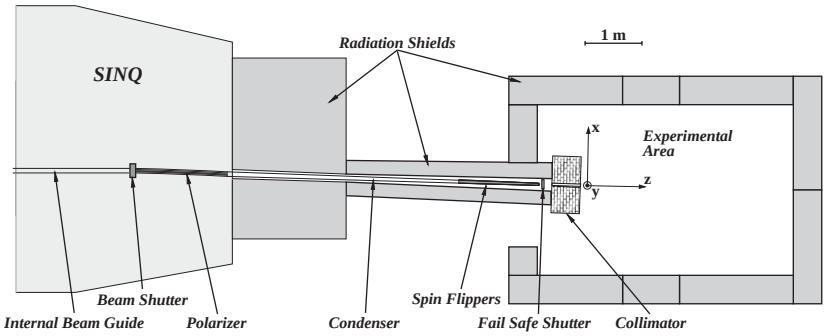

Fig. 1. Schematic top view of the FUNSPIN facility. The coordinate system used in this work is drawn at the position of the experimental apparatus.

guide the collimator is equipped with a vertical guiding magnetic field of around 10–20 G to guide the neutron polarization. During the regular runs of the *R*-correlation experiment neutrons travel through the collimator and through the experimental area in helium atmosphere. The measurements presented in this work, however, were made in air, and its influence was either compensated for by calculated corrections or neglected, if the corrections were very small.

2.1. Neutron beam intensity

The intensity of the neutron beam is proportional to the current of the proton beam impinging on the spallation neutron source target and therefore this quantity will be always given per 1 mA of the proton beam current (at present the typical proton beam current is between 1.0 and 1.2 mA).

The total neutron beam intensity was measured using a gold-foil irradiation method. Because the cross-section for cold neutron capture is proportional to the reciprocal of the neutron velocity and the gold foils were almost transparent to the neutron beam, the measured activity of ^{198}Au is directly proportional to the spatial neutron density. Gold foils with diameter of 25 mm and with two different thicknesses (8 and 20 μm) were placed a few centimeters behind the fail-safe shutter and irradiated for a few minutes. The time of irradiation (at least 1 min) was defined with an accuracy of 1 s by opening and closing the shutter. The spectra of the irradiated gold foils were measured using a germanium detector. Ref. [8] contains a detailed description of that measurement.

The cold neutron beam spatial density measured in the center of the beam is $\rho_0 = (2.95 \pm 0.04) \times 10^3\,\mathrm{cm^{-3}\,mA^{-1}}$, while the neutron flux density is $\Phi = (2.46 \pm 0.04) \times 10^8\,\mathrm{cm^{-2}\,s^{-1}\,mA^{-1}}$ corresponding to a neutron thermal-equivalent flux of $\Phi_{\mathrm{eq}} = (6.49 \pm 0.10) \times 10^8\,\mathrm{cm^{-2}\,s^{-1}\,mA^{-1}}$. Because of the SINQ target upgrade performed in the meantime [9], the measured intensity is significantly higher (by about 23%) in comparison to the one obtained during commissioning of the neutron guide [2].

2.2. Wavelength distribution of the beam intensity

The wavelength distributions of the neutron beam intensity were measured using the time-of-flight (TOF) method. After leaving the collimator the neutron beam is split into bursts by a chopper. Neutrons are detected 1.7 m downstream by a cylindrical, 3 cm diameter and 27 cm long, proportional counter filled with a gas mixture containing ^{3}He. The detector axis is placed horizontally, perpendicularly to the beam direction. Every 20 ms the chopper opens and simultaneously sends a START signal to the Multiscaler Analyzer (MSA). The pulses from the neutron detector are counted in the corresponding MSA time channels. The collected time spectrum consists of 511 channels, each 17.5 μs wide. Since the efficiency of the detector is inversely proportional to the neutron velocity and the detector is nearly transparent to the neutron beam, the measured TOF spectra are directly proportional to the neutron spatial-density distribution.

The measured neutron density distribution is shown in Fig. 2 together with the one from Ref. [2] taken just after commissioning of the neutron guide.[1] For the sake of comparison we normalized the previously measured spectrum to have the same area as the present one since the neutron beam intensity was increased by the upgrade of the spallation target in the source. Both the present and the previous spectrum were treated in the same way: we subtracted background and applied small but necessary corrections described in the next subsection. One can notice that both spectra are very similar in shape. The present density distribution is a little bit harder than the previous one, which might be caused by aging effects of the supermirrors.

2.2.1. TOF spectrum corrections

In order to calibrate the time zero-position we collected TOF spectra with the neutron detector placed at different distances behind the chopper. The measured spectra (Fig. 3) were then

[1] In Fig. 13 of Ref. [2], the spectrum is described as a flux density distribution instead of a density distribution, which seems to be an obvious error.

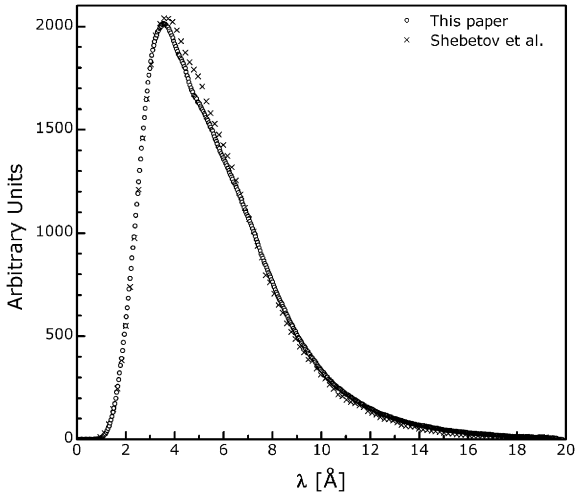

Fig. 2. Wavelength distribution proportional to the neutron beam spatial density. The dots show the present result while the crosses represent the spectrum published by Shebetov et al. [2]. The earlier spectrum was normalized to have the same area as the present one.

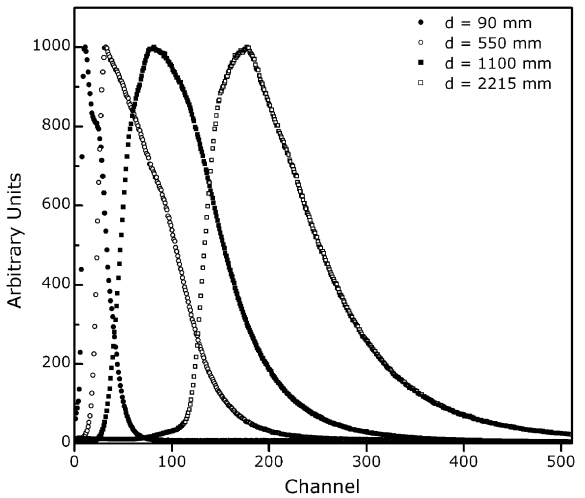

Fig. 3. TOF spectra measured for four distances d (indicated in the figure) between the chopper and the neutron detector. The extrapolation of these spectra to $d = 0$ enables one to determine the absolute zero position of the TOF spectrum.

extrapolated to the distance equal to zero, at which the beam TOF distribution must begin in the first channel. The obtained time offset of 7 channels is in very good agreement with the result of calculations based on the chopper geometry.

The neutron beam burst is produced by an overlap of two slits (rotating and static) and therefore has an almost trapezoid-like time profile: the overlap area increases during 160 μs, then remains constant for 40 μs and finally decreases again during 160 μs. The measured TOF spectra are convolutions of wavelength distributions of neutrons with the beam-burst time profile. In order to study the influence of this convolution a simple simulation assuming the described beam-burst time profile, the Maxwellian neutron velocity distribution and the known distance of 1782 mm between the chopper and the detector was performed. As a result of such integration a shift of about −13 channels is observed as compared to the original Maxwellian distribution; the introduced broadening of the spectrum is less than one time channel. Calculations performed for different temperatures (from 10 to 50 K) of the Maxwellian distribution all led to the same result.

After leaving the neutron guide the neutrons must travel through 2.7 m of air and pass the 0.5 mm thick ^{3}He detector steel housing. The beam attenuation in the air was calculated using the total interaction cross-sections taken from the ENDF Library [10]. The influence of the detector vessel was measured experimentally by placing a second, exactly the same but empty, vessel in front of the active detector. Each measured TOF spectrum was divided channel-by-channel by the appropriate correction factors.

2.3. Neutron beam regular distribution

Two methods were used to determine the angular distribution of neutrons in the beam. The first method used the same apparatus as in the TOF measurements and addressed only angles in the vertical plane. The second method was based on radiography imaging. Knowledge of the beam angular distribution is necessary to calculate the mean value of the polarization (see next section).

In the first method two horizontal slits of 1 mm were mounted on both the chopper and the ^{3}He neutron detector. The angle and the position over the beam cross-section were selected by setting heights of the detector and of the chopper. Fig. 4 shows the angular distributions for four

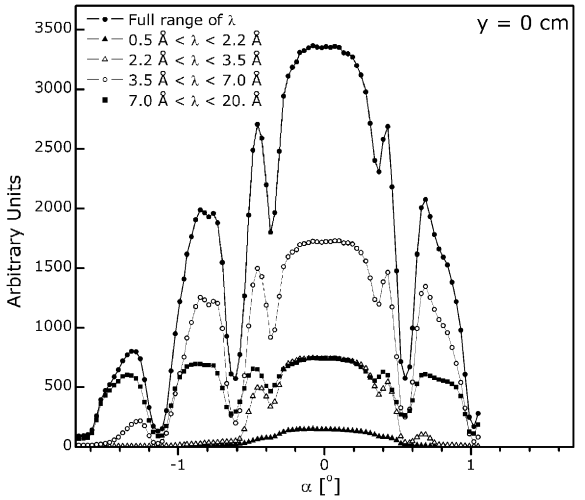

Fig. 4. Vertical angular distribution of the neutrons in the center of the beam ($y = 0$ cm). The distributions for different ranges of the neutron wavelength λ are shown together with the total distribution for relative intensity comparison.

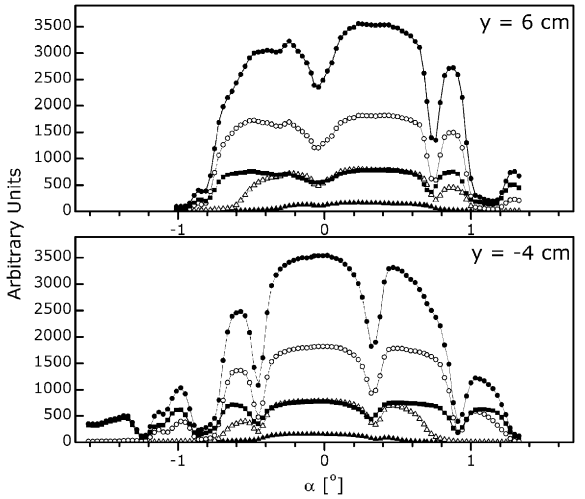

Fig. 5. The same as in Fig. 4 but for the higher ($y = 6$ cm) and lower ($y = -4$ cm) positions of the chopper slit. The same symbols as in Fig. 4 are used to present angular distributions of different neutron wavelength ranges.

wavelength ranges measured at the vertical position $y = 0$ cm of the chopper slit, which corresponds to the center of the beam. The angular range for a given neutron wavelength range agrees very well with the corresponding critical reflection angle $\gamma_{cr}(\lambda)$ of the supermirrors, e.g. mean value of γ_{cr} for $2.2\,\text{Å} < \lambda < 3.5\,\text{Å}$ is equal to 0.56° [2]. Some approximately symmetric minima are visible. Similar structures are reproduced also for the higher ($y = 6$ cm) and lower ($y = -4$ cm) positions of the chopper slit—see Fig. 5.

A similar distribution was obtained using an imaging plate.[2] The plate was placed 380 cm behind a diaphragm with a 5 mm diameter hole at the beam center ($y = 0$ cm). Fig. 6 shows a two-dimensional angular distribution together with its projections on both horizontal and vertical axes. The vertical projection is compatible with the distribution obtained with the first method (Fig. 4). It is worth noting that the radiography method is a much faster tool to determine the angular distribution but it would have to be combined with a velocity selection in order to allow for the full wavelength dependent information.

The positions of the minima visible in the neutron angular distribution are independent of the neutron wavelength; only the range of the angular distribution depends on it (Figs. 4 and 5). The minima are caused by the geometry of the neutron guiding system. Namely, the neutron guide can be traveled only by neutrons entering it with momenta almost parallel to the neutron guide walls. The neutrons can reflect from those walls making reflected images of the neutron guide entrance in their angular distribution at the end of the neutron guide. Fig. 7 shows two example classes of neutron trajectories. The dependence of the measured angular distributions of neutrons on both the geometrical parameters of the system and the critical reflection angle γ_{cr} is clearly visible. All such neutron classes contribute to the whole angular distributions and create observed in the spectra structures which are separated by minima. These minima are smaller or even disappear for neutrons traveling through longer guides, like those installed on the other side of the neutron SINQ target (e.g. Sector 10), which are four times longer. The polarizer, where the neutrons must reflect at least once from the vertically placed supermirrors, decreases the influence of that effect on the horizontal angular

[2]Type: BAS-ND 2040, Fujifilm.

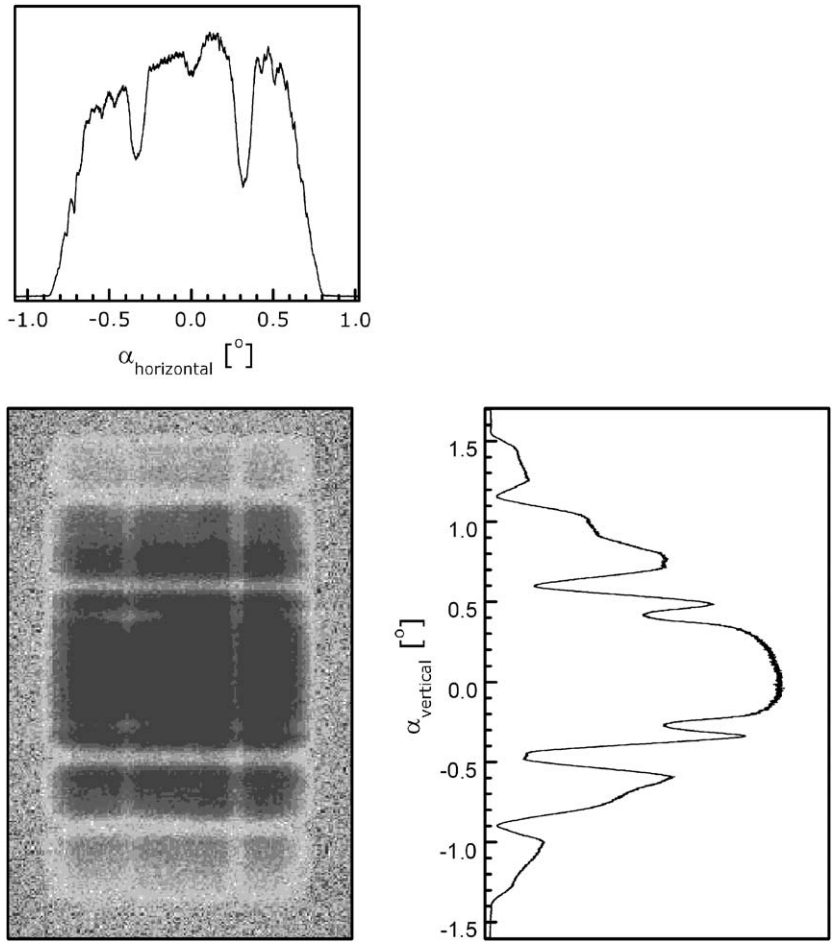

Fig. 6. Angular distribution of the neutrons measured using an imaging plate placed 380 cm behind an aperture with a 5 mm diameter hole in the middle of the beam cross-section. Both horizontal (top panel) and vertical (right panel) projections are shown. The right panel is to be compared with Fig. 4.

distribution. In order to qualitatively check the origin of the visible structures, calculations with the ray-tracing McStas simulation package [11] were performed. For a given model of the SINQ neutron source and for a known geometry of the neutron guide and polarizer it was found (Fig. 8) that structures similar to the measured ones appear if the neutron polarizer is present in the neutron guide but that they are much more pronounced in the horizontal direction if there is no polarizer. The calculations produce the same structures in the vertical neutron angular distribution for both configurations.

2.4. Beam divergence

Another important piece of information to optimize the position of the experimental apparatus is the knowledge of the beam divergence in both vertical and horizontal directions.

For the measurement of the horizontal beam divergence the gold foil irradiation technique was applied. Thin, 12 cm wide and 1 cm high gold foils were irradiated at several distances (10, 40, 70 and 100 cm) from the neutron guide exit. The foil activity distribution was measured using a radiation sensitive imaging plate. One obtains a digital

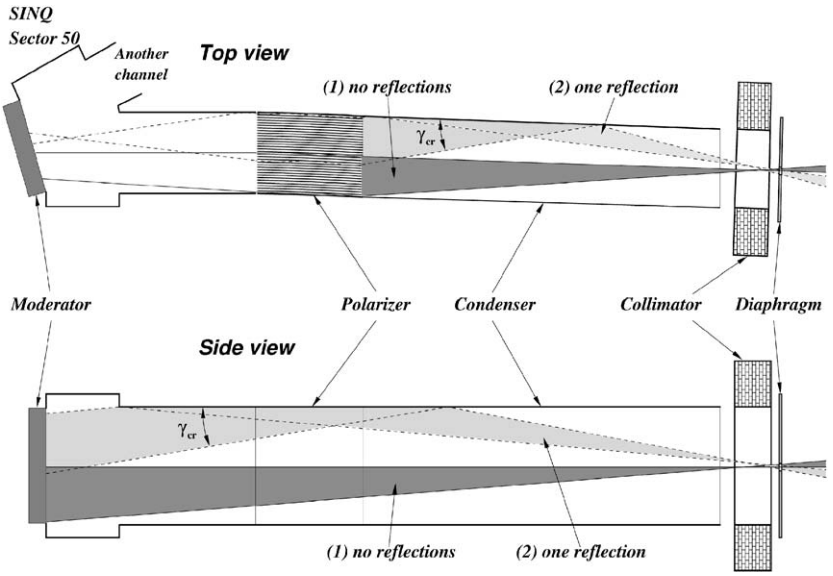

Fig. 7. Schematic view of the neutron guide. Shadowed areas mark ranges of possible trajectories of two example neutron classes which (1) do not reflect or (2) reflect once from the walls. One can observe that the angular distributions of the neutrons measured behind the diaphragm depend on both geometrical conditions and critical reflection angle γ_{cr}. All such neutron classes contribute to the angular distributions shown in Fig. 6. The figure is not to scale. The beam shutter, the fail-safe shutter, the spin flippers and the radiation shields are omitted.

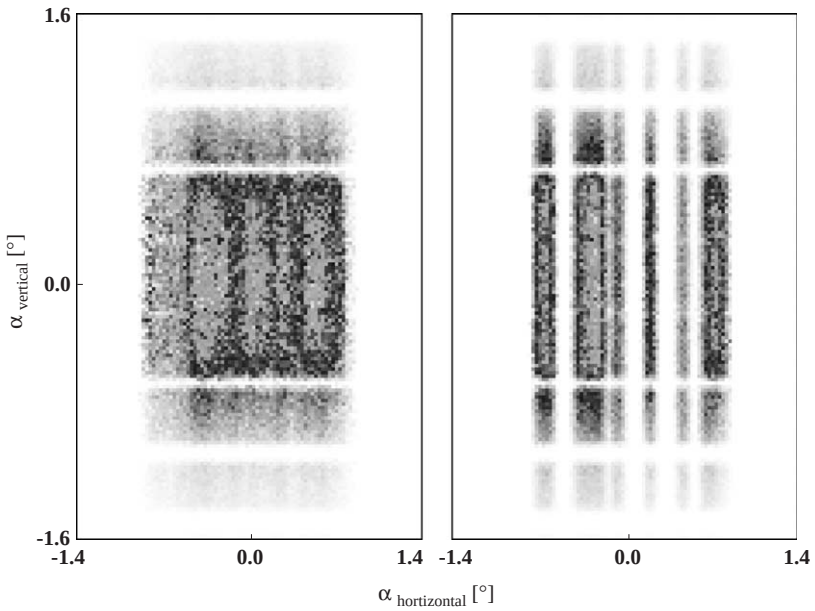

Fig. 8. Angular distribution of neutrons calculated for the center of the beam by the McStas simulation program with (left panel) and without (right panel) the polarizer present in the neutron guide. The left image is to be compared with the measured two-dimensional spectrum from Fig. 6.

image of the irradiated foil convoluted with the resolution function because radiation coming from a certain point of the foil irradiates the imaging plate in some vicinity of that point. This effect was measured at the edge of the foil and was then deconvoluted from the distribution of the foil irradiation. Fig. 9 shows horizontal profiles of the neutron beam taken at different distances from the collimator. The spectrum measured at $d = 10$ cm was convoluted with an assumed divergence spectrum, in which the width was set to reproduce the measured spectra for $d = 40$, 70 and 100 cm. The divergence found in this way is equal to 0.8° with a systematic uncertainty of 0.1° [8]. This result agrees very well with the maximal angle of neutrons in the horizontal angular distribution (Fig. 6, top panel).

The above result allows an estimate of the maximal vertical divergence of the neutron beam on the basis of the vertical projection of the angular distribution (Fig. 6, right panel). That distribution is not symmetric around zero (see also Figs. 4 and 5) and therefore the vertical divergence was estimated separately for upward and downward directions yielding 1.6° and 1.3°, respectively. The systematic uncertainties are estimated by analogy with the ones for the horizontal divergence to be about 0.1°. The observed up–down asymmetry is caused either by the minor geometrical misalignment of the beam line or by the aging effects of the supermirrors.

2.5. *Influence of the beam structure on neutron imaging*

As it was mentioned above the neutron beam leaves the collimator having $45 \times 145\,\text{mm}^2$ cross-section. Fig. 10 shows the neutron radiographic

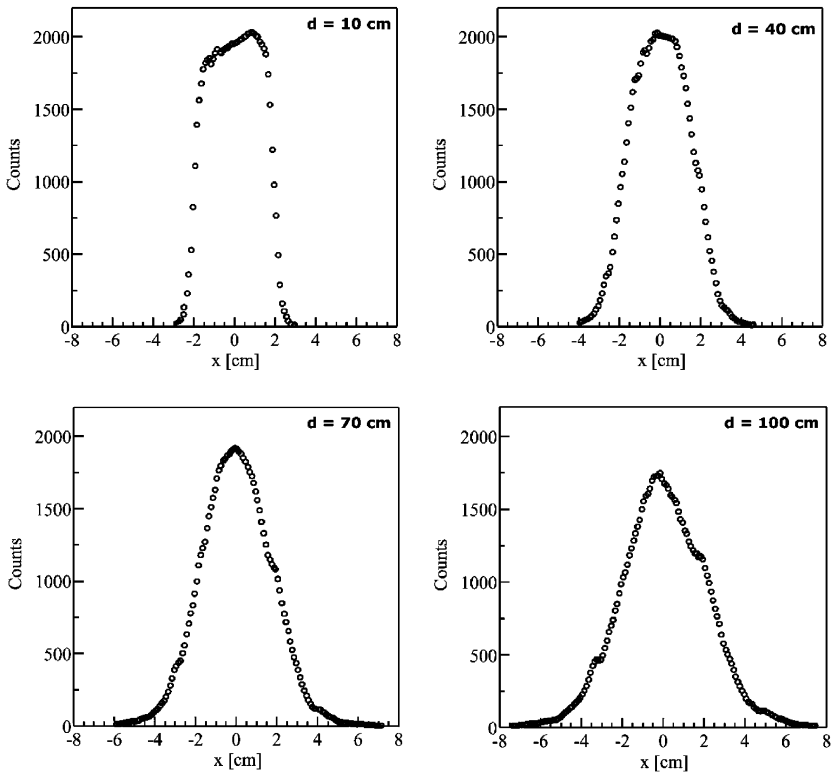

Fig. 9. Horizontal profiles of the neutron beam for different distances d from the collimator exit obtained by the gold foil irradiation technique.

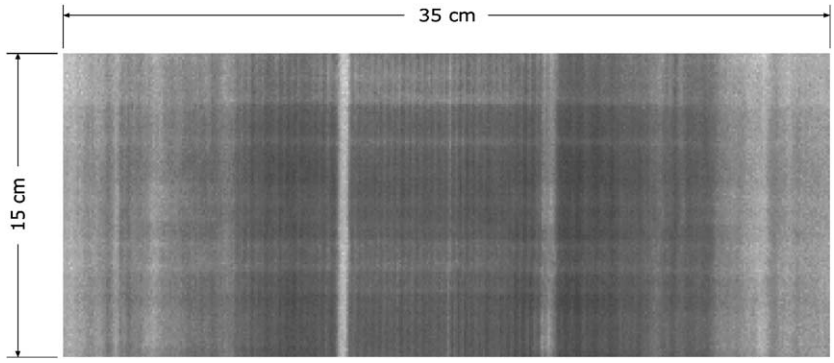

Fig. 10. Neutron radiographic image given by a 1 mm pinhole. The fine structure is due to the multichannel structure of the beam polarizer while the overlying coarse structure originates from the supermirror guide walls.

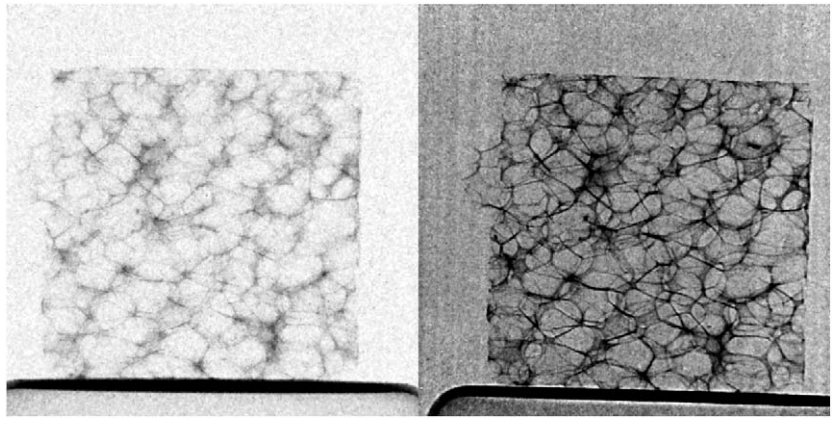

Fig. 11. Image of an aluminum foam ($4 \times 4 \times 1\,cm^3$ plate) made with thermal (left) and cold (right) neutron beams.

image [7] obtained with an imaging plate placed behind a 1 mm pinhole (*camera obscura* method). One can observe a fine structure which is due to the multichannel structure of the beam polarizer and an overlying coarse structure of the supermirror guide walls. Fig. 11 shows an image of an aluminum foam obtained with an uniform thermal neutron beam of the Neutron Transmission Radiography (NEUTRA) facility at SINQ source at PSI (left panel) and of the presented cold neutron beam (right panel). One can notice a much better contrast in the case of the cold neutron radiography image, but on the other hand, one can observe disturbing structures (vertical streaks) on both sides of the sample image, which could create a real problem in case of bigger samples.

3. Beam polarization

A detailed description of both the method and the device used to measure the cold-neutron beam polarization is given in Ref. [12]. Below only the most important features and formulae are recalled and the method of calculating the average beam polarization is presented.

3.1. Polarimeter

A schematic side view of the experimental setup is shown in Fig. 12. The last section of the neutron guide is equipped with two spin flippers (F_1 and F_1') which in this case are considered as the first part of the polarimeter.

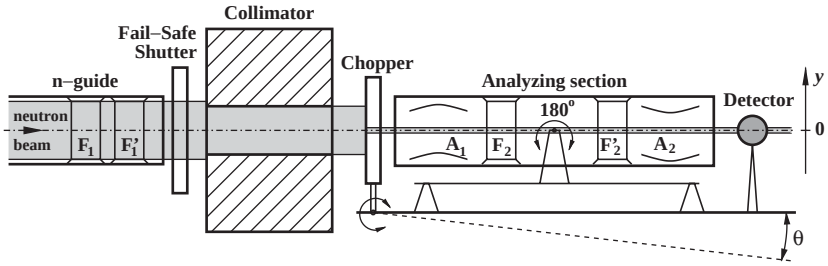

Fig. 12. Schematic side view of the experimental setup for the neutron beam polarization measurement. The shaded area along the horizontal axis indicates the neutron beam. The figure is not to scale. Symbols are described in the text.

The main part of the polarimeter is mounted on a movable support and consists of the chopper, of an analyzing section and of the ^{3}He-filled neutron detector. The support is equipped with a mechanism to change the height y and the inclination angle θ of the apparatus. The analyzing section consists of two polarizers, A_1 and A_2, which are placed at both ends and of two spin flippers F_2 and F'_2 placed between the polarizers. The analyzing section can be rotated through 180° (changing the sequence from $A_1F_2F'_2A_2$ to $A_2F'_2F_2A_1$) to calculate the neutron beam polarization with the use of the super-ratio method [12]. Due to its construction the analyzing section is sensitive to the horizontal polarization component, transverse to the neutron momentum, while the spins of the neutrons in the beam line are oriented vertically. Therefore, a certain distance of about 0.5 m has to be left between the collimator and the chopper to allow an adiabatic rotation of the neutron spins in the magnetic field which changes their direction from vertical to horizontal. The analyzed beam area is defined by a narrow horizontal slit (1 mm wide and 60 mm long) which was mounted on the chopper. The pulses from the detector (after appropriate discrimination) are counted in the multichannel analyzer (Multiscaler), which collects a TOF spectrum of 511 time channels, each 17.5 μs wide. Simultaneously, to correct for the variations of the neutron beam intensity due to variations of the primary proton beam, a similar spectrum of the proton beam current is collected and used for normalization.

TOF spectra (i.e. neutron density distributions) $N^{F'_1F'_2}_{F_1F_2}$, normalized to the proton beam, were collected for 9 states of the flippers: N^{00}_{00}, N^{00}_{10}, N^{00}_{01}, N^{10}_{00}, N^{01}_{00}, N^{00}_{11}, N^{11}_{00}, N^{10}_{10}, N^{01}_{01}, where 0 and 1 indicate the "off" and "on" state of the given flipper, respectively. The spectra were collected for both direct ($A_1F_2F'_2A_2$) and inverted ($A_2F'_2F_2A_1$) positions of the analyzing section. Quantities corresponding to the inverted position are marked by a tilde placed over the quantity symbol, e.g. $\tilde{N}^{00}_{11}$.

The spin-flipper efficiencies f are calculated for each of the four flippers according to the following formulae

$$f_1 = \frac{N^{10}_{10} - N^{00}_{10}}{N^{00}_{00} - N^{10}_{00}} \quad f'_1 = \frac{N^{10}_{10} - N^{10}_{00}}{N^{00}_{00} - N^{00}_{10}}$$
$$f_2 = \frac{N^{01}_{01} - N^{00}_{01}}{N^{00}_{00} - N^{01}_{00}} \quad f'_2 = \frac{N^{01}_{01} - N^{01}_{00}}{N^{00}_{00} - N^{00}_{01}}. \qquad (1)$$

The wavelength distributions of flipper efficiencies measured for the central part of the beam are shown in Fig. 13. Such distributions were calculated for both direct and inverted positions of the analyzing section for each pair of coordinates (y, θ) at which the polarization measurements were performed. These efficiencies are very close to 1 for nearly the whole wavelength range. It was checked that less efficient operation of the spin flippers in certain wavelength ranges does not affect the polarization measurement because of the super-ratio method, which causes such effects to cancel (at least in first-order).

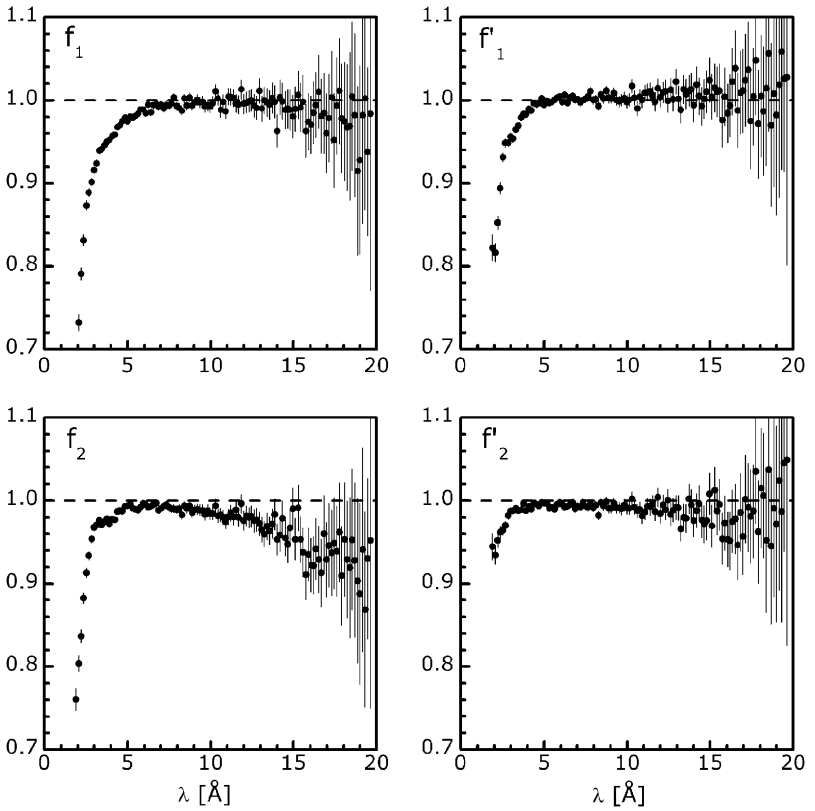

Fig. 13. Wavelength dependencies of the spin flipper efficiencies f_1, f'_1, f_2 and f'_2 measured at the position $y = 0$ cm and $\theta = 0^\circ$ of the polarimeter.

3.2. Polarization and analyzing powers

The polarization and other auxiliary quantities can be calculated using only one pair of flippers: F_1 and F_2 or F'_1 and F'_2. The measurements were performed using both pairs, thus allowing to check the consistency of the results. Final results were calculated by averaging the values obtained with each pair of flippers.

Eight linearly independent quantities are calculated for the pair of flippers F_1F_2, four for the direct position of the analyzing section

$$\begin{aligned} N_{++} &= (N_{00}f_1f_2 + N_{10}f_2) + (N_{01}f_1 + N_{11}) \\ N_{+-} &= (N_{00}f_1 + N_{10}) - (N_{01}f_1 + N_{11}) \\ N_{-+} &= (N_{00}f_2 - N_{10}f_2) + (N_{01} - N_{11}) \\ N_{--} &= (N_{00} - N_{10}) - (N_{01} - N_{11}) \end{aligned} \quad (2)$$

and four for the inverted position

$$\begin{aligned} \tilde{N}_{++} &= (\tilde{N}_{00}\tilde{f}_1\tilde{f}_2 + \tilde{N}_{10}\tilde{f}_2) + (\tilde{N}_{01}\tilde{f}_1 + \tilde{N}_{11}) \\ \tilde{N}_{+-} &= (\tilde{N}_{00}\tilde{f}_1 + \tilde{N}_{10}) - (\tilde{N}_{01}\tilde{f}_1 + \tilde{N}_{11}) \\ \tilde{N}_{-+} &= (\tilde{N}_{00}\tilde{f}_2 - \tilde{N}_{10}\tilde{f}_2) + (\tilde{N}_{01} - \tilde{N}_{11}) \\ \tilde{N}_{--} &= (\tilde{N}_{00} - \tilde{N}_{10}) - (\tilde{N}_{01} - \tilde{N}_{11}) \end{aligned} \quad (3)$$

where the superscripts corresponding to the second pair of the flippers ($F'_1F'_2 = 00$) are omitted. Analogous quantities are calculated for the pair $F'_1F'_2$.

The beam polarization is given by the superratio of the results obtained for the direct and inverted positions of the analyzing section

$$P_A = \left[\frac{N^2_{-+}}{N_{++}N_{+-}} \cdot \frac{\tilde{N}^2_{-+}}{\tilde{N}_{++}\tilde{N}_{+-}}\right]^{1/4}. \quad (4)$$

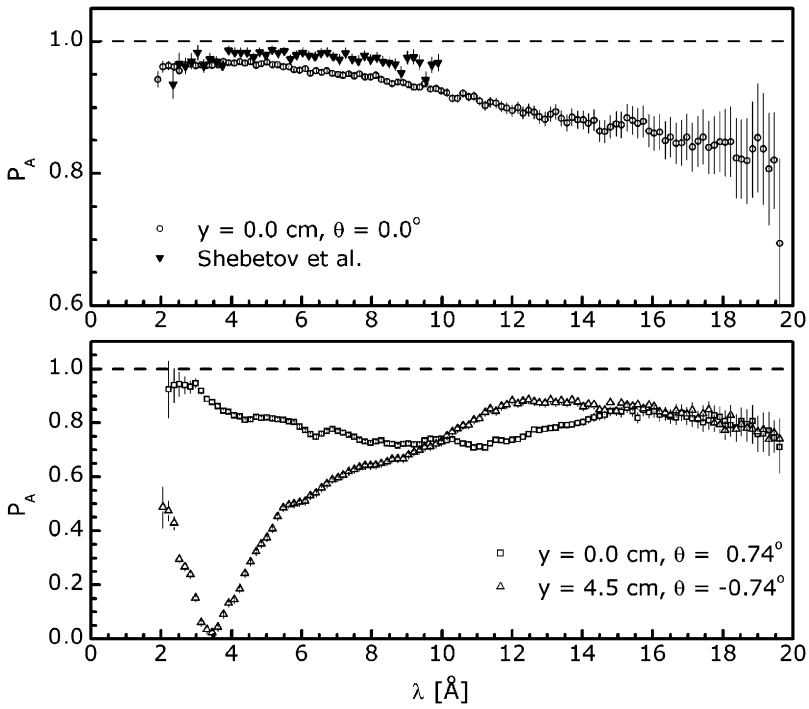

Fig. 14. Wavelength dependence of the polarization P_A measured at the center of the beam for the neutrons traveling horizontally (top panel), and for two other positions of the analyzing section, for which the neutrons had to reflect from the top or bottom walls of the neutron guide to be measured (bottom panel). In addition, the results of the measurement presented in the commissioning paper of the apparatus [2] are shown in the top panel as full triangles. Note the different vertical scales on both panels.

Fig. 14 (top panel) shows the wavelength dependence of the P_A polarization distribution determined for $y = 0\,\text{cm}$ and $\theta = 0^\circ$. The mean polarization for this spectrum over the whole wavelength range is

$$\overline{P}_A(y = 0\,\text{cm}, \theta = 0^\circ) = (95.29 \pm 0.04)\%.$$

As in the case of the TOF spectrum we compare the present results with the ones obtained during the commissioning of the neutron guide in 1999 [2]. The mean value of the formerly measured polarization for the wavelength range from 2 to 10 Å was 97.5% while now we obtain 95.8%. This effect is caused either by some aging effects of the apparatus or due to different measurement conditions. Namely, the former measurement was performed directly at the beam line exit window while the measurement presented here was done about 1.5 m further downstream since the shielding structure and the beam collimator installed meanwhile prevent the polarimeter access to the guide exit window. Moreover, we wanted to measure the neutron beam polarization at the place of the detection system of the R-correlation experiment.

The bottom panel of Fig. 14 shows the results of two other measurements, for neutrons which were at least once reflected from the bottom or top walls of the neutron guide. In this case one can observe significant depolarization effects. Although a reason of this effect is not obvious, one can suppose that both the properties of the supermirrors and the beam line features can generate such effects, e.g. in case of the ($y = 4.5\,\text{cm}$, $\theta = -0.74^\circ$) configuration, neutrons reflect in the area where the spin-flipper begins and where the guiding magnetic field changes its strength by one order of magnitude. It creates a significant field gradients in the vicinity of the supermirror surface what, in turn, can produce neutron depolarization. Fortunately, the amount of such

depolarized neutrons is small and their contribution to the total mean polarization is not sizable. For these two cases the mean polarizations are

$$\overline{P}_{\mathrm{A}}(y = 0\,\mathrm{cm}, \theta = 0.74^{\circ}) = (77.18 \pm 0.04)\%$$

$$\overline{P}_{\mathrm{A}}(y = 4.5\,\mathrm{cm}, \theta = -0.74^{\circ}) = (44.85 \pm 0.04)\%.$$

The errors quoted above are statistical only.

The analyzing powers, describing the quality of the spin analyzers, were calculated for both direct and inverted positions of the analyzing section according to the following formulae:

$$A_1 = \frac{1}{P} \cdot \frac{N_{-+}}{N_{++}}, \quad \tilde{A}_1 = P \cdot \frac{\tilde{N}_{+-}}{\tilde{N}_{-+}}$$
$$A_2 = P \cdot \frac{N_{+-}}{N_{-+}}, \quad \tilde{A}_2 = \frac{1}{P} \cdot \frac{\tilde{N}_{-+}}{\tilde{N}_{++}} \tag{5}$$

where the measured value of P_{A} was inserted in place of the beam polarization P for each measurement point (y, θ, λ). Fig. 15 shows the wavelength dependencies of the analyzing powers of both analyzers and for both positions of the analyzing section. In an ideal case $A_1 = \tilde{A}_1$ and $A_2 = \tilde{A}_2$. Our measurement reveals small (up to 3%) discrepancies for slower neutrons. They have negligible ($< 5 \times 10^{-4}$) influence on the final polarization determination.

Another important quantity describing the performance of the polarimeter is the depolarization coefficient b, which accounts for depolarization of the neutrons due to reflections from the analyzer supermirrors. The b parameter is nearly proportional to a probability of the neutron spin-flip during reflection [12] and depends mainly on material and structure of the supermirror coatings. This coefficient is calculated according to the following formula:

$$b = \frac{1}{4}\left(1 - \sqrt{\frac{N_{--}\tilde{N}_{--}}{N_{-+}\tilde{N}_{-+}}}\right). \tag{6}$$

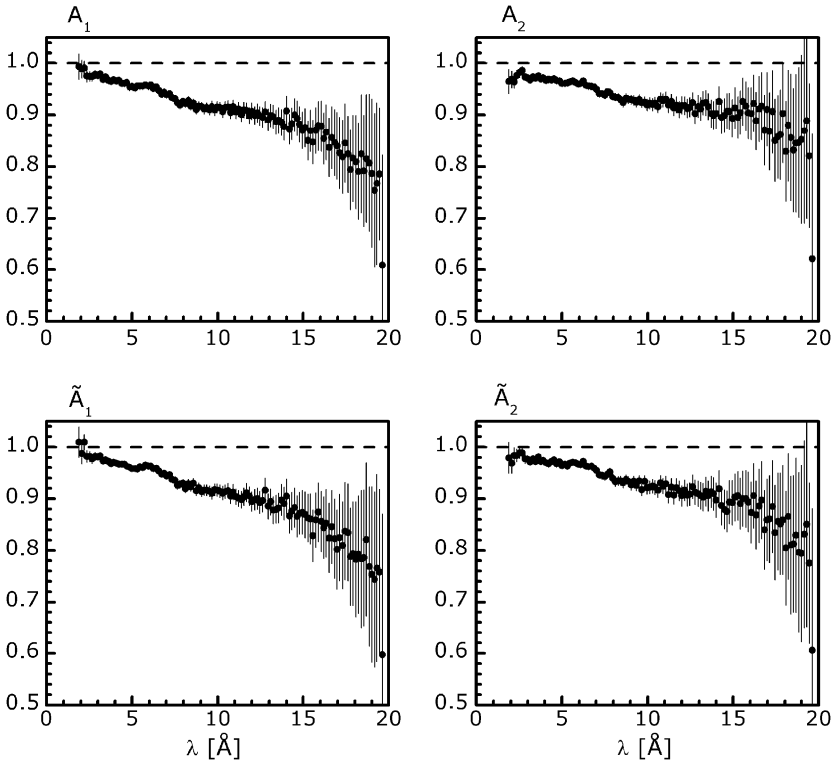

Fig. 15. Wavelength dependencies of the analyzing powers A_1, $\tilde{A}_1$ and A_2, $\tilde{A}_2$ of the analyzers measured at the central position of the beam $y = 0\,\mathrm{cm}$, $\theta = 0^{\circ}$.

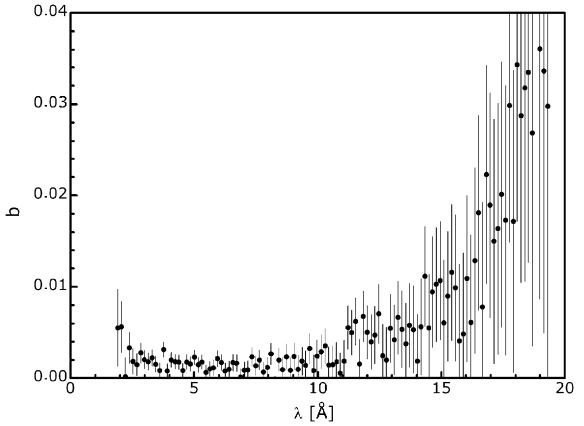

Fig. 16. Wavelength dependence of the depolarization coefficient b for central position of the analyzing section.

A sample spectrum of the depolarization coefficient b, measured at $y = 0\,\mathrm{cm}, \theta = 0^\circ$ is shown in Fig. 16. The mean value in this case is

$$\overline{b} = (1.76 \pm 0.14) \times 10^{-3}.$$

Values of the depolarization coefficient are similar for all measured positions of the analyzing section and are equal to about 2×10^{-3}. The influence of the depolarization parameter on the polarization P_A is less than 10^{-5} and can be neglected.

3.3. Averaging of the neutron beam polarization

The cross-section of the neutron beam is around 145 mm high and 45 mm wide. The range of angles of neutrons in the beam with respect to the beam axis is about $\pm 1.5^\circ$. To calculate the weighted average of the neutron beam polarization it was necessary to perform the polarization measurements for different vertical positions y and inclination angles θ of the polarimeter analyzing section. The measurements were conducted at symmetrical configurations with respect to the central position: $y = 0\,\mathrm{cm}$, $\pm 2.5\,\mathrm{cm}$, $\pm 4.5\,\mathrm{cm}$, $\pm 6.5\,\mathrm{cm}$ and $\theta = 0^\circ$, $\pm 0.37^\circ$, $\pm 0.74^\circ$.

3.3.1. Averaging procedure

In the R-correlation experiment [3] detectors are placed at both sides of the neutron beam and register electrons from the neutron β-decay. In order to calculate the R-coefficient, the beam polarization must be averaged over all neutrons which can emit an electron towards the detection system, that is over the spatial coordinates (x, y, z), vertical and horizontal divergence angles (θ, ζ) and wavelength (λ), with the weights given by the spatial density distribution $\rho(x, y, z, \theta, \zeta, \lambda)$. The design of the polarimeter averages over x and ζ automatically. Here we present an average performed for $z = 0.5\,\mathrm{m}$ (z is the distance between the end of the collimator and the chopper slit), so the variables x, ζ and z are omitted in the spatial density distribution leading to $\rho(y, \theta, \lambda)$. In addition to that spatial-density weight, each measured polarization value is weighted with its statistical uncertainty $\sigma(y, \theta, \lambda)$, and with the fraction $f(y)$ representing the acceptance of the polarization measurement

$$\overline{P}_A = \frac{\int \mathrm{d}y \int \mathrm{d}\theta \int \mathrm{d}\lambda \dfrac{\rho(y,\theta,\lambda) f(y)}{\sigma^2(y,\theta,\lambda)} P_A(y,\theta,\lambda)}{\int \mathrm{d}y \int \mathrm{d}\theta \int \mathrm{d}\lambda \dfrac{\rho(y,\theta,\lambda) f(y)}{\sigma^2(y,\theta,\lambda)}}. \quad (7)$$

The distributions of the weights are discrete because they are obtained from the discrete measurements. Therefore a discretization of the above integrals yields

$$\overline{P}_A = \frac{\sum_i \dfrac{\rho_i \cdot f_i}{\sigma_i^2} \cdot P_A^i}{\sum_i \dfrac{\rho_i \cdot f_i}{\sigma_i^2}} \quad (8)$$

where i goes through vertical positions y, inclinations θ and neutron wavelength values λ.

The 1 mm wide horizontal chopper slit selected only a small fragment of the 145 mm high beam cross-section. Because of time limitations the polarization was measured at only 7 different vertical positions y of the analyzing section. Therefore, the beam cross-section was divided into 7 bins centered around the measurement positions y. The area of each part was used as a fraction-of-the-beam weight $f(y)$, assuming that the polarization is constant for a given bin of the beam cross-section. Extreme values are $f = 0.17$ for $y = 0\,\mathrm{cm}$ and $f = 0.12$ for $y = \pm 6.5\,\mathrm{cm}$.

The measured neutron spatial density distributions are shown in Figs. 4 and 5 as a function of

the neutron vertical position y, of the angle with respect to the horizontal direction α and of the neutron wavelength λ. In order to find the weight ρ one has to integrate the spatial-density distribution within the angular range of the neutrons transmitted through the polarimeter. The transmission of the analyzing section was determined with two 1 mm wide horizontal slits on the entrance of the neutron collimator and on the chopper which selected a portion of the neutron beam with a small angular acceptance: FWHM $= 0.17^{\circ}$. Next, the inclination angle θ of the analyzing section including the neutron detector was changed in several steps. The transmission spectra obtained for the direct and inverted positions of the analyzing section are shown in Fig. 17. These spectra are clearly asymmetric, which might influence the measured polarization values, but the super-ratio method reduces significantly the influence of such asymmetries. One can also notice a strong dependence of the polarimeter transmission on the neutron wavelength λ and on the angle between the analyzing section axis and the neutron flight direction. Knowing the angular dependence enables to define the angular range of neutrons accepted in a particular polarization measurement.

Having determined both the neutron spatial density and the polarimeter transmission distributions one can calculate the neutron-spatial-density weights $\rho(y, \theta, \lambda)$, though the procedure is still ambiguous. The choice of the method giving a possibly small systematic uncertainty of the averaged polarization depends on the features of both the beam and the polarimeter. The influence of different approaches on the final result—the average beam polarization—was tested in a model calculations assuming reasonable beam and polarimeter properties. In that case the mean beam polarization is a priori known.

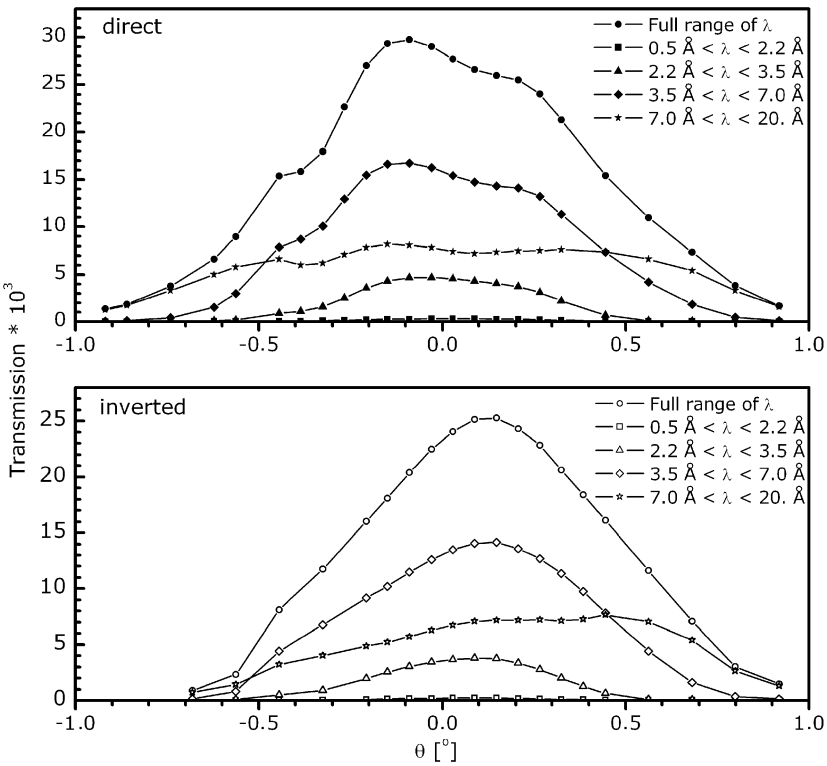

Fig. 17. Transmission spectra of the analyzing section for its direct (top panel) and inverted (bottom panel) positions as a function of the inclination angle θ for all and for selected neutron wavelength ranges.

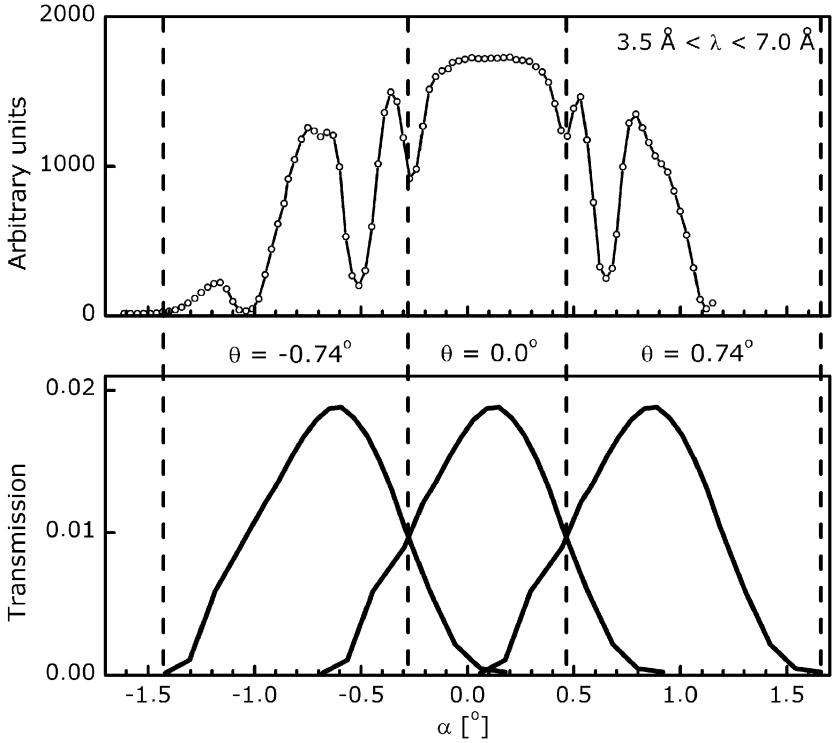

Fig. 18. Illustration of the method used to calculate the spatial density weights ρ_i. Details are given in the text.

Fig. 18 illustrates the best method found for a certain neutron wavelength range λ. One can observe the angular distribution of the neutron beam (open dots in the top panel) and the transmission distributions (thick lines in the bottom panel) for three inclination angles $\theta = 0^\circ, \pm 0.74^\circ$ of the analyzing section. The weights ρ_i are calculated by summing-up the neutron beam angular distribution within the range appropriate for a given θ angle. This range was determined by finding the intersection points of the measured transmission distributions—the limits are marked by dashed, vertical lines in Fig. 18. This procedure was performed for both direct and inverted positions of the analyzing section and, finally, the mean weights ρ_i were calculated.

Because the polarization measurements were performed not only for $\theta = 0^\circ$ and $\pm 0.74^\circ$, but also for $\theta = \pm 0.37^\circ$ it was possible to make an additional check of the method. For this purpose the whole procedure of calculation of the neutron density weights ρ_i was repeated for two ($2P$), instead of three ($3P$), θ-positions of the analyzing section. The result obtained with the second group of measurements ($2P$) should be similar to that obtained with the first one ($3P$) since both groups cover almost the whole range of the neutron beam angular distribution. The $2P$ method, however, introduces larger systematic uncertainties.

The neutron TOF spectrum begins at $\lambda = 1\,\text{Å}$ while the polarimeter is able to measure polarization for neutrons with $\lambda > 2\,\text{Å}$ only (see Figs. 2 and 14). Therefore, the polarization in the non-measurable region had to be extrapolated.

3.3.2. *Average polarization*

Fig. 19 (left panel) shows the total weights $W = \rho f/\sigma^2$ as a function of the vertical position of the analyzing section for inclinations $\theta = 0^\circ, \pm 0.74^\circ$. One can notice the dominance of the horizontally traveling neutrons in the central region of the beam.

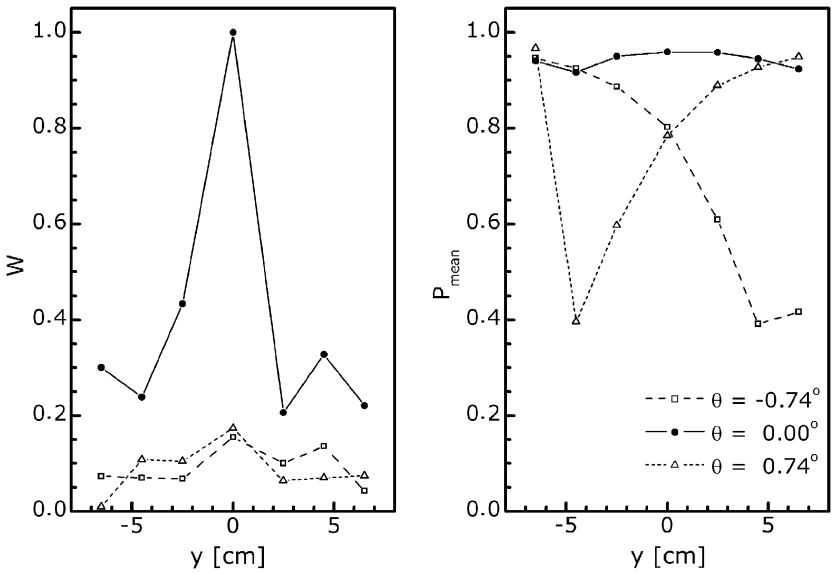

Fig. 19. Left panel—total weights $W = \rho f/\sigma^2$ for all heights and inclinations of the analyzing section. Right panel—dependence of the beam polarization on the height and inclination of the analyzing section of the polarimeter. The same symbols are used for the same inclination angles θ in both panels. The lines are to guide the eye only.

Fig. 19 (right panel) shows the dependence of the beam polarization on the polarimeter position y and its inclination θ. One can notice a high polarization of the neutrons which reflect neither from the top nor from the bottom wall of the neutron guide ($\theta = 0^\circ$) and sizable depolarization effects for the neutrons which are reflected. The neutron polarization for the lowest and highest vertical positions of the analyzing section is relatively high even for the non-zero θ angles but those points have very small weights (see left panel) since only a small number of neutrons follow such trajectories.

Average polarizations calculated using both the $3P$- and $2P$-groups of measurements are

$$P_{3P} = (89.75 \pm 0.01)\%$$
$$P_{2P} = (89.58 \pm 0.02)\%.$$

The errors quoted above are statistical only. The main contribution to the systematic uncertainty originates in the averaging method. As already mentioned, the model calculations were performed to find the optimal averaging method. Those calculations allow also to estimate the maximal systematic uncertainty of the method to be 0.6%. Further uncertainty originates from the extrapolation of the polarization in the non-measurable wavelength region from $\lambda = 1$ to 2 Å. Assuming different reasonable shapes of the extrapolated polarization distribution leads to an estimation of the maximal uncertainty of this extrapolation to be 0.2%. The contribution of less important sources of systematic uncertainty like the fraction-of-the-beam weight f, background subtraction and others is equal to 0.2%. The total systematic uncertainty is then $\Delta = 1.0\%$. Finally, we obtained the average beam polarization

$$P_n = [89.75 \pm 0.01\ (\text{stat}) \pm 1.0\ (\text{syst})]\%.$$

The result obtained using $2P$ method, $P_{2P} = 89.58\%$, lies very well within the limits given by the systematic uncertainty of the averaged beam polarization P_n.

4. Summary

The cold neutron beam line FUNSPIN of the SINQ spallation neutron source at PSI provides

a high flux of polarized cold neutrons—the thermal-equivalent flux is $(6.49 \pm 0.10) \times 10^8\,\mathrm{cm^{-2}\,s^{-1}\,mA^{-1}}$. The neutron beam polarization is high: in the central part of the beam it exceeds 95%. The present result is almost 2% smaller compared to the result obtained during commissioning of the neutron guide and polarizer. This effect may be caused either by aging effects of the apparatus or can be due to different polarization measurement conditions—the present measurement was performed in the area of the detection system of the *R*-correlation experiment, while the former one was performed near to the beam exit window. The weighted average value over the whole beam cross-section is $(89.75 \pm 0.01 \pm 1.0)\%$. The averaged polarization was weighted with the spatial density of the neutrons in the beam what is relevant from the point of view of the *R*-correlation measurement in the decay of free neutrons.

The obtained accuracy of the mean polarization is sufficient from the point of view of the *R*-correlation experiment, however, precise investigations of polarization sensitive observables like the A β-asymmetry coefficient require much smaller systematic uncertainty. This might be achieved either by a more detailed scan of the beam or by applying a ^{3}He spin filter method [13–15].

The efficiencies of two spin flippers which were extracted from the polarization measurement are also important for the *R*-correlation experiment. These efficiencies are very close to 100% for nearly the full wavelength range.

Acknowledgements

This work was performed at the Swiss Spallation Neutron Source SINQ, Paul Scherrer Institute, Villigen, Switzerland. It was supported by the Polish State Committee for Scientific Research under Grant No. 2 P03B 101 22.

The authors would like to express their gratitude to E. Lehmann (PSI) for his help with radiography measurements and to M. Lüthy (PSI) for his help with measurements of absolute neutron flux.

References

[1] W.E. Fischer, Physica B 234–236 (1997) 1208;
G. Bauer, Nucl. Instr. and Meth. B 139 (1998) 65.
[2] A. Shebetov, A. Serebrov, V.M. Pusenkov, M. Lasakov, P. Böni, M. Lüthy, J. Sromicki, Nucl. Instr. and Meth. A 497 (2003) 479.
[3] I.C. Barnett, K. Bodek, P. Boeni, D. Conti, W. Fetscher, M. Hadri, W. Haeberli, St. Kistryn, J. Lang, M. Markiewicz, O. Naviliat-Cuncic, A. Serebrov, J. Sromicki, E. Stephan, J. Zejma, PSI Proposal, June 1997.
[4] J.D. Jackson, S.B. Treiman, H.W. Wyld Jr., Phys. Rev. 106 (1957) 517.
[5] J. Deutsch, P. Quin, in: P. Langacker (Ed.), Precision tests of the standard electroweak model, Advanced Series on "Directions in High Energy Physics", vol. 14, World Scientific, Singapore, 1995, p. 706;
P. Herzog, in: P. Langacker (Ed.), Precision tests of the standard electroweak model, Advanced Series on "Directions in High Energy Physics", vol. 14, World Scientific, Singapore, 1995, p. 786.
[6] K. Bodek, T. Boehm, D. Conti, N. Danneberg, W. Fetscher, C. Hilbes, M. Janousch, S. Kistryn, K. Koehler, J. Lang, M. Markiewicz, J. Sromicki, Nucl. Instr. and Meth. A 461 (2001) 282.
[7] E.H. Lehmann, Proceedings of the 8th Summer School on Neutron Scattering, Zuoz, Publ. World Scientific Publ., Singapore, 2000.
[8] Ch. Hilbes, Ph.D. Thesis, ETH Zürich, No 14458, 2002.
[9] F. Atchinson, H. Spitzer, W. Wagner, 16th Meeting of the International Collaboration on Advanced Neutron Sources, 2003, http://www.fz-juelich.de/ess/Papers/.
[10] Nuclear Data Evaluation Lab, Korea Atomic Energy Research Institute, http://atom.kaeri.re.kr/endfplot.shtml.
[11] A neutron ray-trace simulation package, Risø Nat. Lab. and ILL, http://neutron.risoe.dk/.
[12] A.P. Serebrov, A.V. Aldushchenkov, M.S. Lasakov, I.A. Kuznetsov, I.V. Stepanenko, Nucl. Instr. and Meth. A 357 (1995) 503.
[13] G.L. Jones, T.R. Gentile, A.K. Thompson, Z. Chowdhuri, M.S. Dewey, W.M. Snow, F.E. Wietfeldt, Nucl. Instr. and Meth. A 440 (2000) 772.
[14] D.R. Rich, J.D. Bowman, B.E. Crawford, P.P.J. Delheij, M.A. Espy, T. Haseyama, G. Jones, C.D. Keith, J. Knudson, M.B. Leuschner, A. Masaike, Y. Masuda, Y. Matsuda, S.I. Pentilä, V.R. Pomeroy, D.A. Smith, W.M. Snow, J.J. Szymanski, V.R. Stephenson, A.K. Thompson, V. Yuan, Nucl. Instr. and Meth. A 481 (2002) 431.
[15] O. Zimmer, P. Hautle, W. Heil, D. Hofman, H. Humblot, I. Krasnoschekova, M. Lasakov, T.M. Müller, V. Nisvizhevsky, J. Reich, A. Serebrov, Yu. Sobolev, A. Vassilev, Nucl. Instr. and Meth. 440 (2000) 764.